

OPECAL

D12:ATBD RADIOMETRY MONITORING USING OCEANIC SITES

TECHNICAL NOTE

	Name	Company	Date	Signature
Prepared by :	B. Berthelot	Magellium	29/09/2013	
Checked by :		Magellium		
Approved by :	B. Berthelot	Magellium	29/09/2013	

Document reference :	OPECAL-TN-042-MAG
Issue.Revision :	1.1
Date :	16/12/2014
Client :	ESRIN
Ref., Tender :	AO/1-7043/11/F/MOS

Distribution list

	Name	Company	N. copies
Addresses :	M. Bouvet G. Ottavianelli	ESA/ESTEC ESA/ESRIN	1
Internal copy :	Customer file Project Manager Development team	Magellium Magellium Magellium	1 (digital) 1 (digital) 1 (digital)

Document Change Record

Iss.	Rev.	Date	Reason	Comments
1	0	27/06/2013	Creation of the document	
1	1	16/12/2014	Update of the document	

Table of contents

1 Objectives of the document	7
1.1 Related documents	7
1.1.1 Applicable documents	7
1.1.2 Reference documents	7
1.1.3 Bibliography	8
1.1.4 Acronyms	8
2 Introduction	10
3 Algorithm overview	11
3.1 Principle of the method	11
3.1.1 Method	11
3.1.2 RTM Model	12
3.1.3 6SV	13
3.1.4 Modelling of surface reflectance	13
3.2 Implementation description	14
3.2.1 Overall steps	14
3.2.2 Detailed steps	14
3.2.2.1 Input data selection	14
3.2.2.2 Auxiliary data extraction	15
3.2.2.3 Pixel selection	15
3.2.2.3.1 Sunlint spot avoidance	15
3.2.2.3.2 Clear pixel selection	15
3.2.2.3.3 Valid pixel selection	15
3.2.2.3.4 Foam masking	15
3.2.2.3.5 Aerosol loading	15
3.2.2.4 Gaseous transmission correction	16
3.2.2.5 RTM Solar Irradiance correction	16
3.2.2.6 Aerosol optical thickness estimation in the NIR band	18
3.2.2.7 $\Delta\rho$ estimation in the blue, green, red bands	19
3.2.2.8 Statistical analysis of the sensor radiometry	19
3.2.3 Auxiliary data	19
3.2.3.1 Thresholds	19
3.2.3.2 Generation of LUTS	19
3.2.3.2.1 Constants	20
3.2.3.2.2 NIR LUT used for AOT estimation	20
3.2.3.2.3 LUT 2 : TOA simulation	21
3.2.4 Ancillary data	22
3.3 Spectral bands for which the Calibration is performed	22
4 Dataset analysis to monitor the sensor radiometry using ocean site	23
4.1 Introduction	23
4.2 Site description	23
4.3 Data selection	23
4.4 Analysis of MODIS	24
4.4.1.1 Multiyear results over SIO	24

4.5	Analysis of MERIS.....	25
4.5.1.1	Multiyear results over SIO.....	25
4.6	Analysis of POLDER	26
4.6.1	Multiyear results over SIO.....	26
4.7	Analysis of AASTR	28
4.7.1	Multiyear results over SIO.....	28
4.8	Analysis of ASTR-2	29
4.8.1	Over SIO	29
4.9	Conclusion.....	29
5	Error analysis.....	30

List of the Tables

Table 1: List of applicable documents.....	7
Table 2: List of reference documents	7
Table 3: Solar irradiance	17
Table 4: Spectral band used for AOT retrieval	18
Table 5: Thresholds used to select data.....	19
Table 6: Constant used to select data	20
Table 7: Range of variation of 6SV variables	21
Table 8: Range of variation of 6SV variables	21
Table 9: Ancillary data needed for Rayleigh method.....	22
Table 10: Synthesis of spectral bands in the method.....	22
Table 11: Site Location	23
Table 12: Summary of the Sensor measurement to Simulation measurement ratio.....	29

List of the Figures

Figure 1: Spectral dependence of the aerosol optical thickness for the selected model ..	20
Figure 2: Temporal variability of mean ratio between 2002 and 2011 – BLUE band	24
Figure 3: Temporal acquisition of mean ratio between 2002 and 2011 – GREEN band ...	24
Figure 4: Temporal acquisition of mean ratio between 2002 and 2012 – RED band (645.5 nm)	25
Figure 5: Temporal acquisition of mean ratio between 2002 and 2012 – BLUE band (442.5 nm)	25
Figure 6: Temporal acquisition of mean ratio between 2002 and 2012 – RED band (665 nm)	26
Figure 7: Temporal acquisition of mean ratio between 2002 and 2012 – blue band (443 nm)	26
Figure 8: Temporal acquisition of mean ratio between 2002 and 2012 – blue band (490 nm)	27
Figure 9: Temporal acquisition of mean ratio between 2002 and 2012 – Green band (545 nm)	27
Figure 10: Temporal acquisition of mean ratio between 2002 and 2012 – RED band (670 nm)	27
Figure 11: Temporal acquisition of mean ratio between 2002 and 2012 – Green band (560 nm)	28
Figure 12: Temporal acquisition of mean ratio between 2002 and 2012 – RED band (660 nm)	28

1 Objectives of the document

The purpose of this study is to develop and implement into DIMITRI software a method for monitoring the radiometry of sensors using ocean target.

1.1 Related documents

1.1.1 Applicable documents

Table 1: List of applicable documents

Id.	Ref.	Description
AD1	QA4EO-QAEO-GEN-DQK-001/7, Version 4.0	QA4EO Guidelines (seven documents) http://qa4eo.org/

1.1.2 Reference documents

Table 2: List of reference documents

Id.	Ref.
•	Bouvet M. , Ramoino F., Radiometric intercomparison of AATSR, MERIS, and Aqua MODIS over Dome Concordia (Antarctica), Can. J. Remote Sensing, Vol. 36, No. 5, pp. 464–473, 2010. http://pubs.casi.ca/loi/cjrs
•	DIMITRI Software User Manual ftp://ftp.estec.esa.int/pub/gsp/anonymous/Earth_Observation_Multi-mission_Phase-E2_Operational_Calibration/DIMITRI_SUM.pdf
•	DIMITRI Software Design Document ftp://ftp.estec.esa.int/pub/gsp/anonymous/Earth_Observation_Multi-mission_Phase-E2_Operational_Calibration/DIMITRI_SDD.pdf
•	Statement of Word GSP activity ‘Towards the Intercalibration of EO Medium Resolution Multi-Spectral Imagers’ ftp://ftp.estec.esa.int/pub/gsp/anonymous/Earth_Observation_Multi-mission_Phase-E2_Operational_Calibration/SoW_GSP_TowardsTheIntercomparisonOfEOMediumResolutionMultiSpectralImagers.pdf
•	Hagolle et Al., Results of POLDER in-flight Calibration, IEEE Transactions on Geoscience and Remote Sensing, May 1999, Volume 37, Number 03 [p. 1550]. http://ieeexplore.ieee.org/xpl/RecentIssue.jsp?punumber=36
•	Vermote, E., R. Santer, P.Y. Deschamps and M. Herman, In-flight Calibration of Large Field-of-View Sensors at Short Wavelengths using Rayleigh Scattering, Int. Journal of Remote Sensing, 13, No 18, 1992. http://www.tandf.co.uk/journals/tres

•	Smith D., Poulsen C., Latter B.: Calibration Status of the AATSR Reflectance Channels, MERIS AATSR workshop 2008 proceedings. http://earth.esa.int/meris_aatsr_2008/
---	--

1.1.3 Bibliography

- Ackerman, S. A., K. I. Strabala, W. P. Menzel, R. A. Frey, C. C. Moeller, and L. E. Gumley, 1998: Discriminating clear-sky from clouds with MODIS. *J. Geophys. Res.*, 103 (D24), 32 141–32 157.
- S.Y. Kotchenova, E.F. Vermote, R. Matarrese, & F.J. Klemm, Jr., Validation of a vector version of the 6S radiative transfer code for atmospheric correction of satellite data. Part I: Path Radiance, *Applied Optics*, 45(26), 6726-6774, 2006.
- S.Y. Kotchenova & E.F. Vermote, Validation of a vector version of the 6S radiative transfer code for atmospheric correction of satellite data. Part II: Homogeneous Lambertian and anisotropic surfaces, *Applied Optics*, 2007.
- Morel, Optical modeling of the upper ocean in relation to its biogenous matter content (case I waters), *Journal of Geophysical Research*, 93(C9), 10749-10768, 1988.
- Hagolle, O.; Nicolas, J.-M.; Fougnie, B.; Cabot, F.; Henry, P., "Absolute calibration of VEGETATION derived from an interband method based on the Sun glint over ocean," *Geoscience and Remote Sensing, IEEE Transactions on* , vol.42, no.7, pp.1472,1481, July 2004.

1.1.4 Acronyms

6SV	Second Simulation of a Satellite Signal in the Solar Spectrum, Vector
AATSR	Advanced Along Track Scanning Radiometer
ADEOS	Advanced Earth Observation Satellite
ATSR	Along Track Scanning Radiometer
ATCOR	ATmospheric CORrection
AVHRR	Advanced Very High Resolution Radiometer
BOUSSOLE	BOUée pour l'acquiSition d'une Série Optique à Long termE
BRDF	Bidirectional Reflectance Distribution Function
Cal/Val	CALibration and VALidation
CEOS	Committee on Earth Observation Satellites
CNES	Centre National d'Etudes Spatiales
CVI	Cal/Val interest
DIMITRI	Database for Imaging Multispectral Instruments and Tools for Radiometric Intercomparison
DN	Digital Number
ENVISAT	ENVIronment SATellite
EO	Earth Observation
ESA	European Space Agency
IVOS	Infrared and Visible Optical Sensors
LandNet	Land Network
MERIS	Medium Resolution Imaging Spectrometer

MODIS	Moderate Resolution Imaging Spectroradiometer
MODTRAN	Moderate-Resolution Atmospheric Radiance and Transmittance Model
NASA	National Aeronautics and Space Administration
NOAA	National Oceanic and Atmospheric Administration
PARASOL	Polarization & Anisotropy of Reflectances for Atmospheric Sciences coupled with Observations from a Lidar
POLDER	POLarization and Directionality of the Earth's Reflectances
QA4EO	Quality Assurance Framework for Earth Observation
RADTRAN	Radiative Transfer
RIM	Radiometric Instrument Model
ROSAS	RObotic Station for Atmosphere and Surface
RTM	Radiative Transfer Model
SADE	Structure d'Accueil de Données d'Etalonnage
SNR	Signal to Noise Ratio
SWIR	Short Wave Infra-Red
TOA	Top Of Atmosphere
VGT	VEGETATION
VIS	VISible
WG	Working Group
WGCG	Working Group on Calibration and Validation

2 Introduction

This Algorithm Theoretical Basis Document describes the algorithm used to monitor the sensor radiometry using the Rayleigh scattering over ocean sites. This method is referred by "Rayleigh method". In particular, this document identifies sources of input data, both satellite and auxiliary data. It provides the physical theory and mathematical background underlying the use of this information in the method; It includes implementation details, and describes assumptions and limitations of the adopted approach.

This task is referred by task 3 of the SOW.

The software processes images acquired over the sites by ATSR-2, AATSR, MODIS/Aqua, MERIS, and PARASOL instruments.

3 Algorithm overview

3.1 Principle of the method

The Rayleigh scattering method is a method for the absolute calibration of optical instruments without using in-situ measurements. Absolute calibration is achieved through an absolute calibration of the blue and red spectral bands using the well-characterized Rayleigh scattering signal over ocean.

For a given viewing and solar angles and from the knowledge of the surface pressure, the Rayleigh scattering can be accurately predicted by radiative transfer codes (Teillet, 1995 Hagolle et al., 1999). It may contribute to 90 % of the TOA signal from blue to red bands. The others contributions to the TOA signal are the water-leaving radiance, foam presence, and aerosol amount. The aerosol scattering contribution is retrieved from NIR bands where molecular scattering is negligible (Vermote et al., 1992) and transferred to the short wavelength bands to model the TOA radiance with radiative transfer software. The simulated radiance values are compared to the measured values to derive the absolute calibration coefficient.

To reduce the influence of the water leaving radiance and foam, a pixel selection procedure is applied aiming at chosen the best conditions: Clear water sites, large viewing and sun angles to increase the atmospheric path, and viewing in a westerly direction to avoid specular reflection.

The principle of the method is to compare the measurements provided by the sensor over an ocean site to a simulation of the top-of-atmosphere reflectance (Eq. 1). This ratio is computed for all acquisitions and monitored on a large period of time to detect possible change in sensor radiometry.

$$\Delta\rho = \frac{\rho_{TOA}^{Measured}}{\rho_{TOA}^{Simulated}} \quad \text{Eq. 1}$$

In this ATBD, we will describe the method implemented to monitor the temporal variability of this ratio.

3.1.1 Method

The Top Of the Atmosphere reflectance corrected from the gaseous transmission is modelled as the sum of the reflectance of all contributors to the signal:

$$\rho_{TOA}^{Measured} = \rho_m + \rho_a + \rho_{ma} + (1-f)T_m T_a \rho_{sun} + t_m t_a ((1-f)\rho_w + f \cdot \rho_f) \quad \text{Eq. 2}$$

where ρ_m is the reflectance due to molecular scattering (or Rayleigh scattering), ρ_a is the aerosol reflectance, ρ_{ma} is a multiple scattering term modelling the interaction between aerosols and molecules, ρ_w is the marine reflectance at sea level (i.e. the marine radiance normalised by the solar irradiance at sea level), ρ_f is the foam reflectance at sea level, f is the

pixel fraction covered by foam (the more wind the higher f), $t_m t_a$ is the product of the diffuse transmittances of molecules and aerosols, respectively, along the path Sun to surface and surface to satellite. The reflectance denoted ρ_{sun} is due to the specular reflection of the Sun on sea surface and it is weighted by the direct transmission of the atmosphere from surface to satellite, $T_m T_a$. The coupling between Fresnel reflection and atmospheric scattering is taken into account in the atmospheric terms ρ_m and ρ_a . This linearisation is based on a large-scale formalism, in which adjacency effects are neglected. It is not applicable to pixels contaminated by the presence of land.

The equation above is only valid when gaseous absorption and scattering effects may be decoupled. This is the case for most spectral bands in the visible domain except for the bands in which strong oxygen and water vapour absorption occurs.

Assuming the wind-speed and the marine reflectance known, the first step consists in estimating the aerosol scattering contribution. This is done from TOA reflectances measured in the NIR band where water leaving radiance does not contribute. Outside sunglint and without foam, the apparent reflectance is written as the sum of molecular and aerosol contributions

$$\rho_{TOA}^{Measured} = \rho_m + \rho_a + \rho_{ma} \quad \text{Eq. 3}$$

For this, a radiative transfer code is used to simulate the TOA signal from surface inputs. Results are stored in the form of Look-up tables. These tables are composed of pre-calculated top of the atmosphere reflectances computed for different level of AOT, pressure, water vapour content, wind speed, and a set of illumination and acquisition conditions (view and solar zenith and azimuth angles).

Interpolations are made to the inputs values of the model (angles, water vapour, wind speed, pressure) to obtain a LUT depending only of the AOT. The AOT value which minimizes the differences between the modelled and the observed TOA reflectance is selected.

Then, the TOA reflectances in the other channels are estimated directly using the estimated aerosol optical thickness in the LUT in a direct mode.

The ratio of measured to simulated reflectance in spectral bands lower than 670 nm are computed and monitor with time.

3.1.2 RTM Model

We choose to use 6SV1 RTM to perform the simulations and estimate all terms of equation 2.

6SV1 RTM is a reference model used to perform accurate simulations of the solar radiation reflected by the surface-atmosphere system as measured by satellite and plane observation, accounting for elevated targets, use of anisotropic and lambertian surfaces and calculation of gaseous absorption. The code is based on the method of successive orders of scatterings approximations and is able to account for radiation polarization (Kotchenova et al., 2006; Kotchenova and Vermote, 2007).

Simulations are performed for all spectral bands of the reference sensor, the geometrical illumination and observation conditions, an atmosphere described by an aerosol model and an optical thickness, an atmospheric profile depending on the latitude, water vapor and ozone content, a wind speed and a water leaving reflectance.

- 1) 6S allows the coupling between ocean and atmosphere.
- 2) A water leaving reflectance model is available in 6S (Morel, 1988). It depends on chlorophyll concentration level.

At least there are two possibilities to simulate the TOA reflectances.

1) Method 1 : Direct modelling using RTM

The method runs the RTM in a direct way for the set of selected inputs. The comparison is performed directly.

This solution is probably the best because it does not introduce methodological errors but is not applicable due to the computation time.

2) Method 2: Use pre computed Look Up Tables of output of RTM

The method is based on the use of Look Up Tables containing simulated TOA reflectances for a large range of variations of the inputs parameters and the search the actual configuration which is closest to the simulation.

3.1.3 6SV

The RT 6S code is code used for simulating satellite and plane observations, accounting for elevated targets, use of anisotropic and Lambertian surfaces, and calculation of gaseous absorption.

The 6S code is based on the method of successive orders of scattering (SOS) approximations. Within this method, the atmosphere is divided into a number of layers and the RT equation is solved numerically for each layer with the help of iterations. The intensity is successively computed for photons scattered one, two, three times, and etc. with the total intensity obtained as the sum of all orders. Numerical integration is performed using the decomposition in Fourier series for the azimuth angle and Gaussian quadratures for the zenith angle.

The complete 6SV validation effort is summarized in two manuscripts:

- S. Y. Kotchenova, E. F. Vermote, R. Matarrese, and F. Klemm, Validation of a vector version of the 6S radiative transfer code for atmospheric correction of satellite data. Part I: Path Radiance, Applied Optics, 45(26), 6726-6774, 2006.
- S. Y. Kotchenova and E. F. Vermote, Validation of a vector version of the 6S radiative transfer code for atmospheric correction of satellite data. Part II: Homogeneous Lambertian and anisotropic surfaces, Applied Optics, 2007.

Remark:

6SV does not allow to account for pressure variation directly. A correction has been proposed and added to the processing according to Gordon and Wang, XXX.

The correction is applied on the molecular reflectance.

3.1.4 Modelling of surface reflectance

6S has a module which allows the computation of the BRDF of an ocean surface by taking into account the influence of whitecaps, sun glint and pigment concentration.

The surface reflectance is estimated from the three following components:

- 1) the reflectance due to whitecaps $\rho_{wc}(\lambda)$,
- 2) the specular reflectance at the ocean surface $\rho_{sg}(\lambda)$,
- 3) the scattered reflectance emerging from sea water $\rho_{sw}(\lambda)$

Contributions 1 and 3 are removed in the selection of the scene is performed according to a selection based on wind speed.

Models are detailed in 6S user manual.

3.2 Implementation description

3.2.1 Overall steps

This paragraph provides with the overall steps that have to be done to estimate the absolute coefficient calibration.

- 1) Read the database and select images acquired in the site.

For each selected date (loop)

- 2) Read the TOA reflectances of clear pixels acquired into the site footprint for the selected date.
- 3) Read auxiliary data
 - 3.1) Wind speed
 - 3.2) Water vapour content
 - 3.3) Ozone content
 - 3.4) Pressure
 - 3.5) Chlorophyll concentration
- 4) Check Pixels selection test
 - 4.1) Select clear pixels
 - 4.2) Apply test on wind speed
 - 4.2.1) Select pixels such as Windspeed < 5m/s
- 5) Correct TOA reflectances from gaseous absorption
- 6) Estimate Aerosol optical thickness in the NIR band
- 7) Estimate ρ TOA using the estimated AOT in band to calibrate
- 8) Estimate the reflectance ratio in the short wave bands (blue to red)

3.2.2 Detailed steps

3.2.2.1 Input data selection

DIMITRI data ingestion module allows to extract for each acquisition the area. One file is written for one acquisition. According to the period selected by the user, these files are read and used as input of the method.

The output file of the ingestion module contains the following information:

- Latitude;
- Longitude;
- Zenith and azimuth solar angles;
- Zenith and azimuth view angles;
- TOA reflectance in all channels;
- Cloud mask ;

3.2.2.2 Auxiliary data extraction

Water vapour content, ozone content and wind speed are extracted from ERA dataset for the location of data which contains the site. The data are provided each 6 hours. A linear interpolation is performed to estimate the different content at the hour of acquisition.

3.2.2.3 Pixel selection

The selection of pixels to perform absolute calibration method is the first step of the processing. The calibration data selected to maximize the atmosphere contribution to the measured signal corresponds to the following criteria:

- No sunglint contribution;
- No clouds;
- No foam.

If the following criteria are not validated, the method could not apply for the selected pixels.

3.2.2.3.1 Sunglint spot avoidance

An automatic selection removing acquisitions for which sunglint spot is present is performed based on the estimation of the reflected sun angle threshold θ_r .

$$\cos(\theta_r) = \cos(\theta_s)\cos(\theta_v) + \sin(\theta_s)\sin(\theta_v)\cos(d\phi)$$

Where θ_s is the solar zenith angle and ϕ_s the azimuth angle; θ_v is the viewing zenith angle and ϕ_v the azimuth angle. $d\phi = \phi_s - \phi_v$

Rayleigh processing path is taken when the reflected sun angle, θ_r , is higher than 36° .

3.2.2.3.2 Clear pixel selection

The clear pixels found in the site location are selected to apply the methodology. The cloud mask is computed in the ingestion procedure, and stored in the acquisition extract. The clear pixel detection is described in the cloud detection ATBD.

Clear pixels are selected.

3.2.2.3.3 Valid pixel selection

It must be noted that Level 1 quality indicators have been used to discard pixels from the processing. Saturated/Invalid flagged pixels are removed.

Valid pixels are selected.

3.2.2.3.4 Foam masking

To avoid foam contamination, pixels is selected if the wind speed is lower than the defined threshold (around 5 m/s). The threshold has been proposed by Hagolle et al., 2004.

Pixels for which wind speed is lower than 5 m/s are selected.

3.2.2.3.5 Aerosol loading

Aerosol loading is estimated in the NIR band. A threshold of 0.1 on the value of the inverted AOT is applied to limit the uncertainty on the aerosol model chosen to simulate the TOA reflectances. AOT greater than the threshold are removed from the processing.

Pixels for which AOT is lower than 0.1 are selected.

3.2.2.4 Gaseous transmission correction

The comparison of the measured reflectance to the estimated one is performed on data corrected from the gaseous transmission. Therefore, it is necessary to estimate the gaseous transmission for each pixel selected by the previous selection step.

The gaseous transmission has been estimated using SMAC formulation.

Analytical formulation is used to simulate the gaseous transmission from the air mass, gaz content (water vapour content, ozone content) and surface pressure. The formulation has been developed first by Rahman and Dedieu, (1996), then improved by Berthelot and Dedieu (2000). SMAC coefficient database has been developed for all optical sensors on orbit up to 2008 by B. Berthelot and is made available for free on CESBIO web site. The coefficients are estimated for H₂O, O₃, O₂, CO₂, CH₄, NO₂, CO gaz.

Input for total gaseous transmission estimation is :

- ✦ Solar zenith angle
- ✦ View zenith angle
- ✦ Water vapour content
- ✦ Ozone content
- ✦ Pressure
- ✦ SMAC coefficients for all bands

Output is :

- ✦ Total Gaseous transmission.

3.2.2.5 RTM Solar Irradiance correction

The comparison of the TOA reflectance to the simulated one is not direct unless the transformation of radiances to reflectances is performed using the same solar irradiance reference. Indeed, the sensors record raw digital numbers (DN) that are related to the radiances with a sensor radiometric model that can be more or less complex. Once all parameters of this radiometric model estimated, the radiance can be estimated from the measured digital numbers. Then, the TOA reflectances are computed from radiances using the conversion:

$$\rho_{TOA}^k = \frac{\pi L^k}{E_{os}^k \left(\frac{d_o}{d}\right)^2 \cos(\theta_s)} \quad \text{Eq. 4}$$

Where k refers to the spectral band, E_{os} is the solar extraterrestrial irradiance in the spectral band k, (d_o/d) is the ratio of Sun-Earth distance at the acquisition date to the mean Sun-Earth distance, and θ_s is the solar zenith angle.

The use of a RTM allows to simulate the apparent reflectance at the satellite level. This reflectance is modelled by:

$$\rho_{6S-TOA}^k = \frac{\pi L^k}{E_{os-6S}^k \left(\frac{d_o}{d}\right)^2 \cos(\theta_s)} \quad \text{Eq. 5}$$

Where for this case E_{os-6S} is the 6S solar extraterrestrial irradiance in the spectral band k. 6S solar irradiance reference is Neckel and Labs, 1984.

In order to compare both TOA reflectances, the measured reflectance has to be weighted by the ratio of the solar extraterrestrial irradiance

$$\rho_{6S-TOA}^k = \rho_{TOA}^k \times \frac{E_{os}^k}{E_{os-6S}^k} \quad \text{Eq. 6}$$

The 6S solar irradiances are reported hereafter for each spectral band in a table where the solar irradiance used for the transformation of radiances to radiances are also provided. The corrective factor is indicated in the last column.

Table 3: Solar irradiance

Sensor	Band number	Central wavelength [nm]	E_{os} sensor (W/m ²)	E_{os-6S} (W/m ²)	E_{os} / E_{os-6S}
MODIS	1	645	1578.11	1603.89	0.984
MODIS	2	858.5	971.74	992.78	0.979
MODIS	3	469	2058.78	2012.55	1.023
MODIS	4	555	1838.69	1859.45	0.989
MODIS	5	1240	454.67	453.66	1.002
MODIS	6	1640	239.77	237.82	1.008
MODIS	7	2130	98.85	95.25	1.038
PARASOL	1	443	1891.16	1897.41	0.997
PARASOL	2	490	1928.39	1935.50	0.996
PARASOL	3	565	1843.69	1842.30	1.001
PARASOL	4	670	1527.45	1532.73	0.997
PARASOL	5	763	1225.40	1229.75	0.996
PARASOL	6	765	1228.45	1232.41	0.997
PARASOL	7	865	980.89	980.40	1.000
PARASOL	8	910	885.09	929.03	0.953
PARASOL	9	1020	712.50	726.33	0.981
MERIS	1	412.5	1716.09	1735.08	0.989
MERIS	2	442.5	1880.34	1858.00	1.012
MERIS	3	490	1929.82	1924.68	1.003
MERIS	4	510	1930.42	1916.12	1.007
MERIS	5	560	1804.47	1845.70	0.978
MERIS	6	620	1652.05	1700.73	0.971
MERIS	7	665	1532.81	1547.51	0.991

MERIS	8	681.25	1473.30	1495.47	0.985
MERIS	9	708.75	1409.03	1394.20	1.011
MERIS	10	753.75	1267.02	1262.78	1.003
MERIS	11	760.625	1255.55	1242.03	1.011
MERIS	12	778.75	1178.17	1192.53	0.988
MERIS	13	865	959.12	972.21	0.987
MERIS	14	885	930.56	975.05	0.954
MERIS	15	900	896.15	943.92	0.949
AATSR	1	560	1819.54	1853.11	0.982
AATSR	2	660	1521.89	1546.01	0.984
AATSR	3	862	950.68	971.14	0.979
AATSR	4	1593	254.48	253.03	1.006
VGT	1	460	1963.40	1972.01	0.996
VGT	2	670	1570.30	1551.73	1.012
VGT	3	825	1045.60	1058.47	0.988
VGT	4	1640	234.70	228.24	1.028
ATSR2	1	554			
ATSR2	2	658			
ATSR2	3	864			
ATSR2	4	1608			

3.2.2.6 Aerosol optical thickness estimation in the NIR band

The algorithm estimates the AOT using the LUT of the reference spectral band such as the simulated TOA reflectance is equalled to the observed one. Then, the AOT is used to estimate the TOA reflectance that should be measured in the other bands.

The reference bands used for AOT retrieval are:

Table 4: Spectral band used for AOT retrieval

Sensor	Spectral band used for wind speed retrieval
MODIS	Band 2
MERIS	Band 13
AATSR	Band 3
ATSR2	Band 3
PARASOL	Band 7

3.2.2.7 $\Delta\rho$ estimation in the blue, green , red bands

Once the AOT estimated, the TOA reflectances in the short wave channels are estimated using the LUTs. The search is performed to find the data stored in the LUT which surround the values of the measurements of solar zenith angle, view zenith angle, relative azimuth angle, chlorophyll and AOT in this order. Then the value of the simulated TOA reflectance (normalised to the gaseous transmission) is interpolated between the two last surrounding values at the estimated AOT.

The ratio of TOA reflectances measured out to TOA reflectances estimated is computed for all bands before 0.670 μm .

$$\Delta\rho^{Blue} = \frac{\rho_{toa}^{measured}}{\rho_{toa}^{estimated}}, \quad \Delta\rho^{Green} = \frac{\rho_{toa}^{measured}}{\rho_{toa}^{estimated}}, \quad \Delta\rho^{red} = \frac{\rho_{toa}^{measured}}{\rho_{toa}^{estimated}} \quad \text{Eq. 7}$$

As the algorithm is applied on a pixel per pixel basis, a statistical analysis on calibration coefficients will be made to remove outliers. Mean and standard deviation of the ratio are estimated and values out of three σ are removed.

3.2.2.8 Statistical analysis of the sensor radiometry

The last step consists in averaging the values of the ratio obtained for one acquisition and monitor it with time.

$$\overline{\Delta\rho} = \text{mean}\left(\frac{\rho_{TOA}^{Measured}}{\rho_{TOA}^{Simulated}}\right) \quad \text{Eq. 8}$$

3.2.3 Auxiliary data

3.2.3.1 Thresholds

The following thresholds have to be defined:

Table 5: Thresholds used to select data

Name	Threshold value
Wind speed (m/s)	5
Reflected Sun angle (degrees)	36
Minimum of AOT	0.05

3.2.3.2 Generation of LUTS

To apply the method, two Look up tables are computed using the new vectorial version of 6S (6SV, Kotchenova et al., 2007). The first one is dedicated to the aerosol optical thickness estimation. The second one is dedicated to the simulated TOA reflectance computation.

3.2.3.2.1 Constants

The choice of the **aerosol model** is, as recommended by Hagolle et al., 2004, the M98 model, corresponding to a maritime model with 98% humidity. The spectral dependency is represented hereafter:

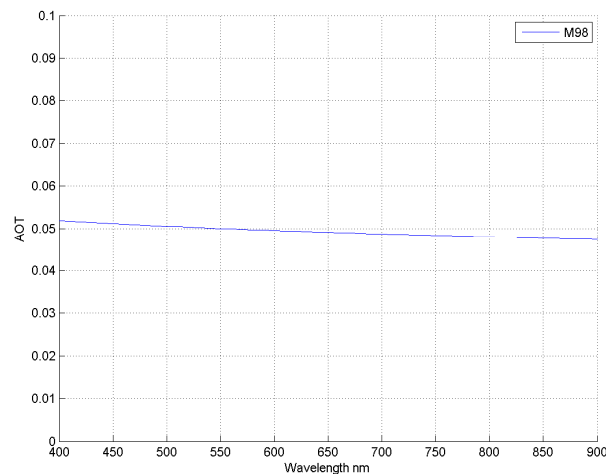


Figure 1: Spectral dependence of the aerosol optical thickness for the selected model

DIMITRI sites, located in the South Pacific Gyre and South Indian Ocean, are inside oligotrophic geographic areas having a priori well-known weak and stable chlorophyll content (oligotrophic waters).

Cox and Munk constant variable

In the model, the **sea surface salinity** is set to 34 PSU.

The refraction index is estimated for the spectral bands based on this salinity. It estimates the index of refraction of sea water (n_r) and the extinction coefficient of sea water (n_i)

Table 6: Constant used to select data

Name	Constant value
Aerosol type	M98
SSS	34 PSU
Wind azimuth	0

3.2.3.2.2 NIR LUT used for AOT estimation

For the NIR band a LUT is created for the estimation of the apparent TOA reflectance. This LUT will be a function of sun zenith angle, view zenith angle, relative azimuth angle, water vapour and AOT.

The sampling is adapted to each sensor, based on the configuration observed on acquisitions. It is reported in the tables below:

Table 7: Range of variation of 6SV variables

	Range	Step	Number of values
sun zenith angle	[0 – 70] degrees	5 degrees	13
view zenith angle	[10 – 70] degrees	5 degrees	13
Solar azimuth	[0 – 180] degrees	5 degrees	37
View azimuth	0	0	1
AOT	[0.01 0.04 0.07 0.1]		4
Water vapour content	[0.5 -4.5] g/cm ²	0.5	5
Ozone	0.3 cm.atm	0	1
[Chl. a]	0.05 mg/m ⁻³	0	1
Wind Speed	2 m/s	0	1

3.2.3.2.3 LUT 2 : TOA simulation

For the spectral bands located in the short wave, LUTs are also created to estimate the apparent TOA reflectance. In this case, the chlorophyll concentration varies, based on the values observed on auxiliary dataset. These LUTs are a function of sun zenith angle, view zenith angle, relative azimuth angle, wind speed, water vapour, chlorophyll concentration and AOT.

The sampling is reported in the table below:

Table 8: Range of variation of 6SV variables

	Range	Step	Number of values
sun zenith angle	[10 – 70] degrees	5 degrees	13
view zenith angle	[0 – 60] degrees	5 degrees	13
Solar azimuth	[0 – 180] degrees	5 degrees	37
View azimuth	0	0	1
AOT	[0.01 0.04 0.07 0.1]		4
Water vapour content	[0.5 -4.5] g/cm ²	1	5
Ozone	0.3 cm.atm	0	1
[Chl. a]	[0.02 0.06 0.1] mg/m ⁻³	-	3
Wind Speed	2 m/s	0	1

3.2.4 Ancillary data

Water vapour content and ozone content are taken from the ERA interim datasets. ERA-Interim is a global atmospheric reanalysis from 1979 to present. Global atmospheric and surface parameters from 1 January 1979 to present, at T255 spectral resolution (~80 km) on 60 vertical levels are available. For this study, 6-hourly atmospheric fields on water vapour content, ozone content, and wins speed have been downloaded from 2001 to year 2012 from the ECMWF Data Server.

Table 9: Ancillary data needed for Rayleigh method

Data	Source
Water vapour content	ECMWF
Ozone content	ECMWF
Wind speed	ECMWF
Pressure	ECMWF
Chlorophyll concentration	Globcolour

3.3 Spectral bands for which the Calibration is performed

This table summarises the sensor spectral bands for which the method is applied.

Table 10: Synthesis of spectral bands in the method.

Wave_Centre	AATSR	ATSR2	MERIS	MODISA	PARASOL
412			0		
443			1		0
470				3	
490			2		1
510			3		
530					
555	0	0	4	4	2
620			5		
665	1	1	6	1	3
681					
708					
750					
761					
765					
778					
830					
860					
870	2	2			6
885			13	2	

4 Dataset analysis to monitor the sensor radiometry using ocean site

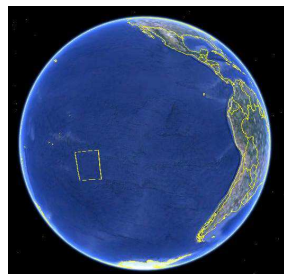
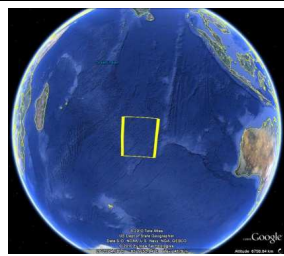
4.1 Introduction

This section provides the results of the method set up to estimate the change in the radiometry over ocean site. The results are provided for all sensors except VEGETATION for all acquisitions available in the database. Only data available over SIO site have been processed. The details of the implementation are provided for the processing of one single acquisition. Then, the results are provided for the processing of the data time series

4.2 Site description

This paragraph provides the characteristics of the variability of data used in input of the RTM. It provides also the level of variations that has been used to dimension the LUTS. The variability is plot for the SIO/SPG site location for indication.

Table 11: Site Location

Site name	Location	Illustration
South Pacific Gyre	[-30.5 S, -31.0 S, -129.0 W, -129.5 W]	
South Indian Ocean	[-30.0 S, -30.5.0 S, 80.0 E, 80.50 E]	

4.3 Data selection

The dataset analysis aims to identify the acquisitions which will be suitable to apply the method. The data selection aims to select acquisitions such as :

$$\theta_r > 36^\circ$$

4.4 Analysis of MODIS

4.4.1.1 Multiyear results over SIO

The change in sensor radiometry is estimated by computing the mean of the measured to simulated TOA reflectances ratio for all available acquisitions. It is represented for the three MODIS bands (465.5nm, 553 nm, and 645.5 nm) in the figures below.

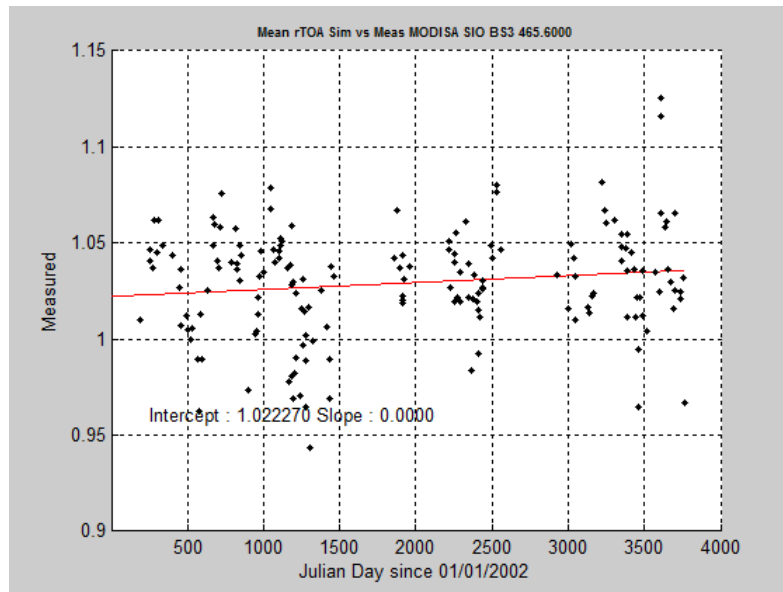


Figure 2: Temporal variability of mean ratio between 2002 and 2011 – BLUE band

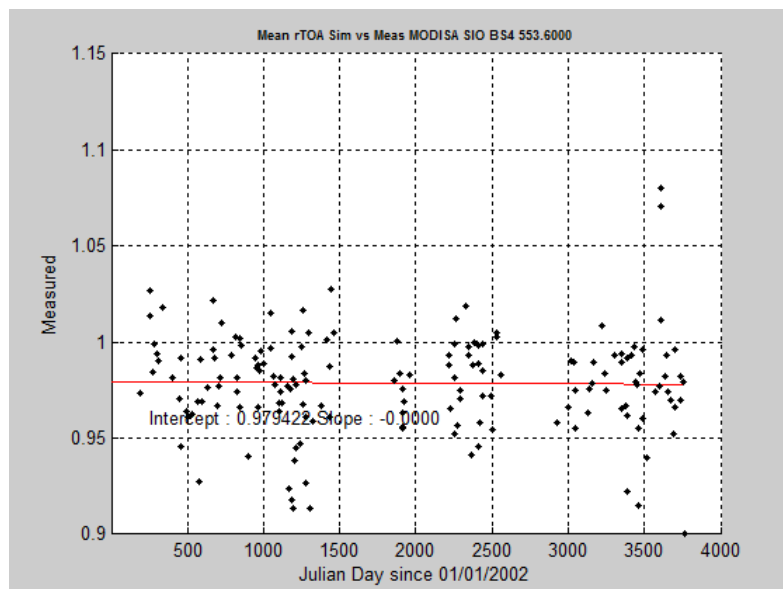


Figure 3: Temporal acquisition of mean ratio between 2002 and 2011 – GREEN band

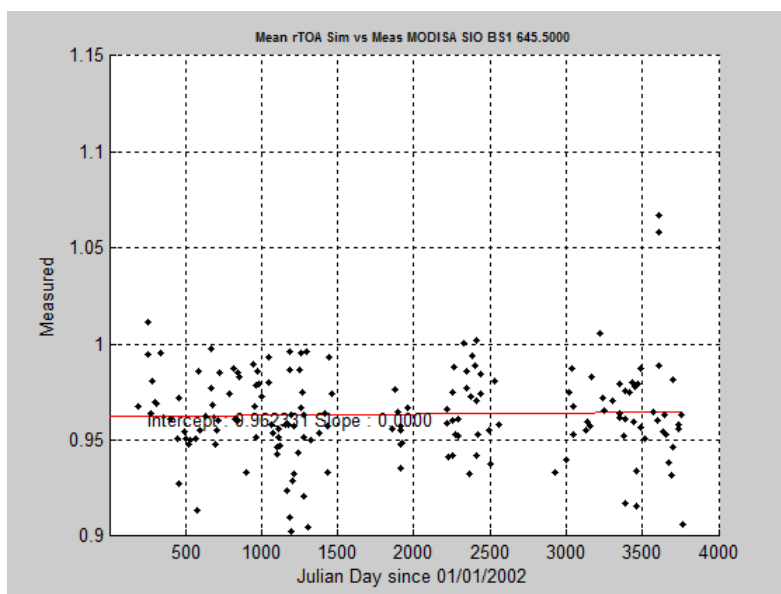


Figure 4: Temporal acquisition of mean ratio between 2002 and 2012 – RED band (645.5 nm)

4.5 Analysis of MERIS

4.5.1.1 Multiyear results over SIO

The change in sensor radiometry is estimated by computing the mean of the measured to simulated TOA reflectances ratio for all available acquisitions. It is represented for the three MODIS bands (442.5 nm and 665 nm) in the figures below.

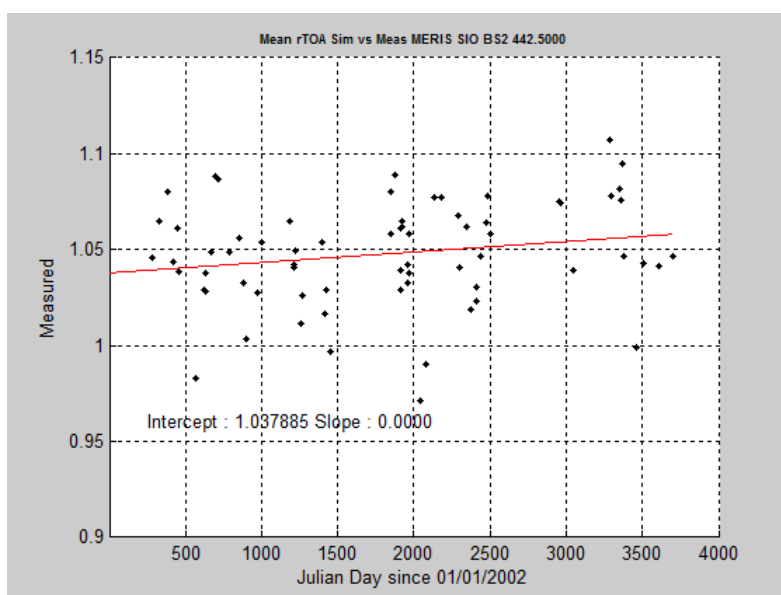


Figure 5: Temporal acquisition of mean ratio between 2002 and 2012 – BLUE band (442.5 nm)

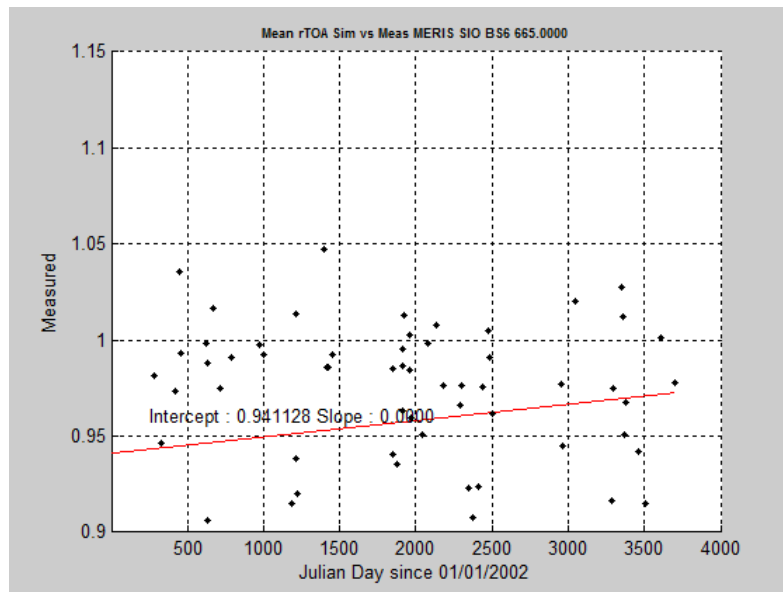


Figure 6: Temporal acquisition of mean ratio between 2002 and 2012 – RED band (665 nm)

4.6 Analysis of POLDER

4.6.1 Multiyear results over SIO

The change in sensor radiometry is estimated by computing the mean of the measured to simulated TOA reflectances ratio for all available acquisitions. It is represented for the three MODIS bands (443 nm, 490 nm, 550 nm and 670 nm) in the figures below.

From the available time series, only a few date match the pixel selection criteria. Results are illustrated for direction 9.

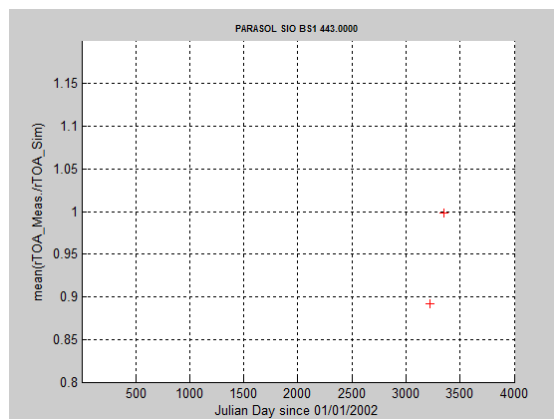


Figure 7: Temporal acquisition of mean ratio between 2002 and 2012 – blue band (443 nm)

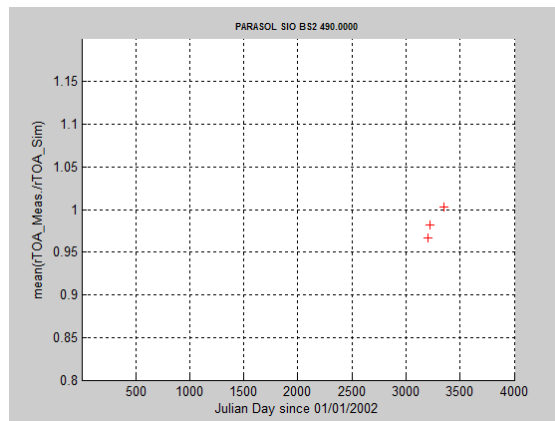


Figure 8: Temporal acquisition of mean ratio between 2002 and 2012 – blue band (490 nm)

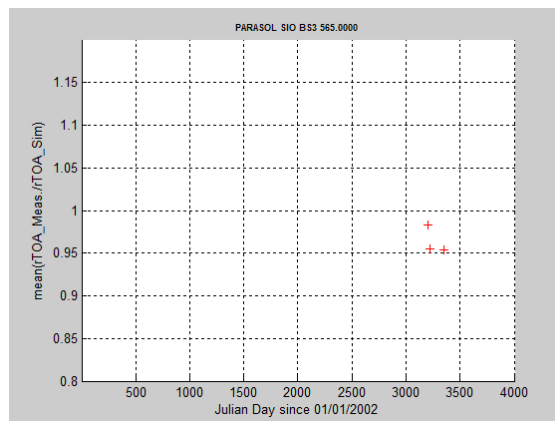


Figure 9: Temporal acquisition of mean ratio between 2002 and 2012 – Green band (545 nm)

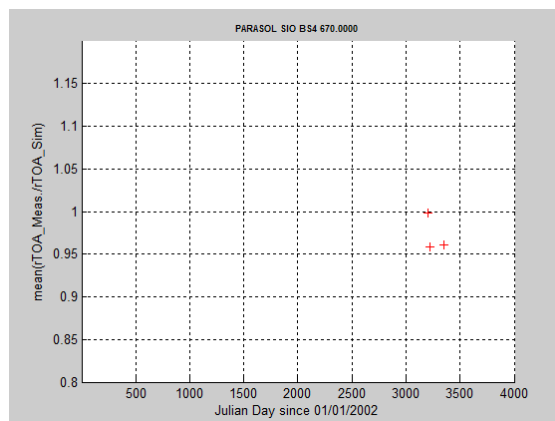


Figure 10: Temporal acquisition of mean ratio between 2002 and 2012 – RED band (670 nm)

4.7 Analysis of AASTR

4.7.1 Multiyear results over SIO

The change in sensor radiometry is estimated by computing the mean of the measured to simulated TOA reflectances ratio for all available acquisitions. It is represented for the three MODIS bands (550 nm and 670 nm) in the figures below.

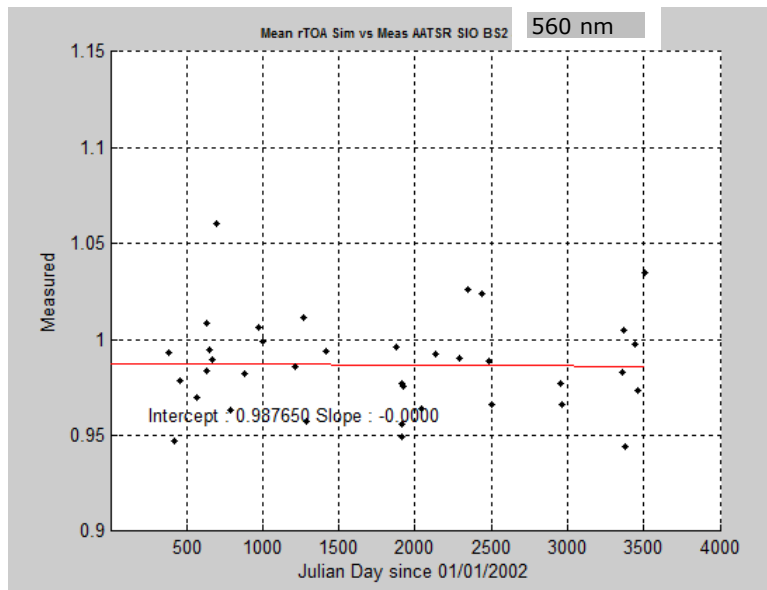


Figure 11: Temporal acquisition of mean ratio between 2002 and 2012 – Green band (560 nm)

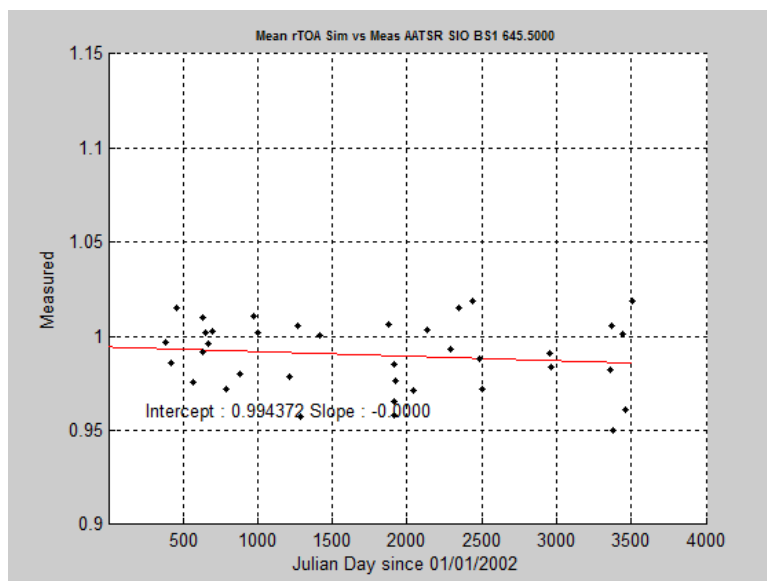


Figure 12: Temporal acquisition of mean ratio between 2002 and 2012 – RED band (660 nm)

4.8 Analysis of ASTR-2

4.8.1 Over SIO

Not processed

4.9 Conclusion

The methodology dedicated to the monitoring of the sensor radiometry has been implemented and tested for all data available, except ATSR-2. Variability of the Sensor measurement to Simulation measurement mean ratio is reported in the next table.

Table 12: Summary of the Sensor measurement to Simulation measurement ratio

Sensor	BLUE	GREEN	RED
MODIS	1.022 at 465 nm	0.979 at 553 nm	0.962 at 645 nm
MERIS	1.037 at 442.5 nm		0.941 at 665 nm
PARASOL	Not enough data	Not enough data	Not enough data
AATSR		0.987 at 560 nm	0.994 at 660 nm

However, a few dates seem still to be not well filtered and request detailed analysis to remove them from the processed temporal series. This can come from the total number of points that is not low, or to the geographic scattering of the selected points on the images.

A correlation with the AOT thickness extracted with MODIS LEVEL3 will be also performed to confirm the AOT retrieval from the LUT, or implement a filter to discard some dates based on the high value of observed AOT.

5 Error analysis

Several authors (Hagolle et al, 1999) for instance have performed detailed error analysis for the sensor calibration using the sun glint method. The following list recaps the main post of uncertainties.

The uncertainties in the method include:

- Uncertainties in the radiative computation: If the solar zenith angle is smaller than 75°, the accuracy of the radiative transfer calculation based on plane parallel approximation is better than 10^{-3} in reflectance units (Vermote and Tanré, 1992).
- Calibration errors: Error on the reference band (NIR band) involves error on the aerosol optical thickness, therefore in the other spectral bands. Error in band calibration is assumed to be 3%.
- Geophysical uncertainties:
 - ❖ Gaseous absorption:
 - ❖ ozone amount : 5%
 - ❖ water vapour amount: 20%
 - ❖ Chlorophyll content. Spectral bands lower than 0.67 μm are affected by errors on chlorophyll content. According to Hagolle et al, 1999, an error of 50% on the chlorophyll concentration leads to an uncertainty on calibration coefficient up to 2% for 443 nm channel.
 - ❖ Rayleigh optical thickness: 1.5 % resulting from an error of 15 hPa on pressure.
 - ❖ Aerosol type: low, 1.5%
 - ❖ Foam is discarded using only pixels where the wind speed is lower than 5m/s.

- End of the document -